Experimental Validation of Low Dispersion and High Birefringence Properties of THz Polymer Porous Fibers

Shaghik Atakaramians[1,2], Shahraam Afshar V.[1], Heike Ebendorff-Heidepriem[1], Michael Nagel[3], Bernd M. Fischer[2], Derek Abbott[2], and Tanya M. Monro[1]

[1] *Centre of Expertise in Photonics, The University of Adelaide, SA 5005 Australia*
shaghik@eleceng.adelaide.edu.au, shahraam.afsharvahid@adelaide.edu.au,
heike.ebendorff@adelaide.edu.au, tanya.monro@adelaide.edu.au
[2] *Adelaide T-ray group, The University of Adelaide, SA 5005 Australia,*
bfischer@eleceng.adelaide.edu.au, dabbott@eleceng.adelaide.edu.au
[3] *Institut für Halbleitertechnik, RWTH Aachen University, 52074 Aachen, Germany*
nagel@iht.rwth-aachen.de

Abstract: The experimental results confirm the low dispersion characteristics of porous fibers compared to microwires and a 0.012 birefringence for 0.65 THz is achieved for porous fiber with asymmetrical air-hole shape.

Introduction: In recent years there has been increased interest in low loss and low dispersion THz waveguides as potential substitutes for the free-space optics in terahertz spectroscopy and imaging systems. A number of waveguide solutions based on technologies from both electronics and photonics, have been studied for guiding THz radiation, among which solid-core sub-wavelength fibers [1] (called THz microwires [2, 3]), air-core microstructured fibers [4, 5], and Ag/PS-coated hollow glass fibers [6] have the lowest loss reported in the literature for dielectric based waveguides. These dielectric waveguide solutions are either large in diameter, which reduces the flexibility of the waveguide, or are only suitable for relatively narrow band applications.

Recently, a novel class of THz fibers, porous fibers, was proposed [7, 8]. These fibers are air-clad fibers that exhibit sub-wavelength air-holes in the core and whose diameters are less or comparable to the operation wavelength. This allows low loss propagation and improved confinement of the field compared to microwires (solid-core sub-wavelength fibers). As theoretically shown [8], porous fibers have a lower dispersion relative to microwires. Moreover, introducing asymmetrical sub-wavelength air-holes in porous fiber leads to a strong birefringence, making these fibers a potential substitute for free space THz propagation where the polarization of the field is preserved [9].

In terms of state of the art in porous fiber fabrication, Dupuis et al. have proposed a subtraction technique [10]. In this method after drawing down the composite preform, the fiber segments were submerged into a solvent for several days to etch away the material residing in holes. The fibers were also left to dry for several days. Although the air-holes were preserved in this method, the fabrication process in very lengthy and the choice of material is limited in terms of dissolving solvent and melting temperature differences between the materials. Large melting temperature differences can result in material degradation. Moreover the maximum porosity achieved was 29-45%.

In this work, to the best of our knowledge, we demonstrate the first fabrication of highly porous (more than 55%) THz fibers. We present the fabrication of polymer porous fibers with two different types of sub-wavelength air-hole shapes: spider-web (symmetrical) and rectangular (asymmetrical). We also confirm experimentally the predicted effective refractive indices of porous fibers, which validate both the low dispersion characteristics of the porous fibers compared to their microwire counterparts and the birefringence characteristics for rectangular porous fiber.

Porous Fiber Fabrication: The polymer material used for the fabrication of porous fibers and microwire is Polymethyl methacrylate (PMMA), whose optical properties in the THz region are reported in Ref. [3]. As a reference, at 0.5 THz, the absorption coefficient and refractive index of the PMMA are 4.2 cm^{-1} and 1.65, respectively. The fibers are fabricated in a two-step process. First the preforms with the macroscopic structure are manufactured using the extrusion technique, which has been demonstrated to be not only viable for soft glasses [11] but also for polymers [12]. The preforms are extruded by heating up a bulk polymer billet to a temperature where the material gets soft (170-

180 ˚C). Then the soft material is forced through an extrusion die using a ram extruder at a fixed speed. The die exit geometry determines the preform cross-section. The die exit geometry and the extruded performs of spider-web and rectangular porous fibers are shown in Fig. 1(a), Fig. 1(b), Fig. 1(d) and Fig. 1(e), respectively.

In the next step, a cut of 180mm from the extruded perform of 10-15 mm diameter and 150cm long is drawn down to bands of more that 10 meters of fibers with outer diameter of 350 μm using a fiber drawing tower. The scanning electron microscope (SEM) images of the cross-section of the spider-web and rectangle porous fibers are shown respectively in Fig. 1(c) and Fig. 1(f). The porosity of the spider-web and rectangular porous fibers given by the die design are 67% and 71%, respectively. Using SEM images, the porosity of the fibers is measured to be 57% and 65%, respectively. This decrease in porosity is due to rounding in the corners and thickening of the struts. We used an extruded polymer optical fiber with a 250μm outer diameter for the THz microwire [4].

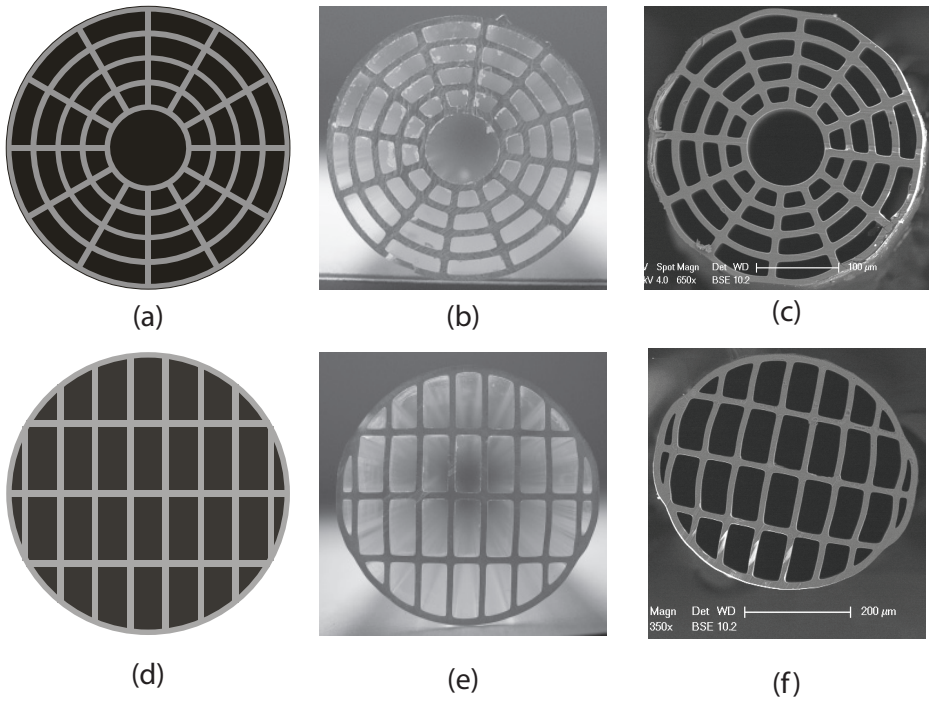

Fig. 1: The die design of the (a) spider-web and (d) rectangular porous fibers. The extruded preforms of the (b) spider-web and (e) rectangular porous fibers. The SEM images of the cross-section of the (c) spider-web and (f) rectangular porous fibers.

THz Experiment: The THz properties of the fabricated porous fibers are investigated using terahertz time domain spectroscopy (THz-TDS). A mode-locked Ti:sapphire laser with a pulse width of less than 170 fs, central wavelength of 800 nm and a repetition rate of 76 MHz is used to drive the emitter and the detector. The fiber tips are positioned as close as possible on the emitter and detector. The emitter is a photoconductive array of antennas [13]. The schematic of the THz-TDS setup is shown in Fig. 2.

Assuming single mode propagation, the equation governing the input and output electric fields of the fiber can be written in the frequency domain as:

$$E_{\text{out}}(\omega) = E_{\text{ref}}(\omega) T_1 T_2 C_2 \exp(-\alpha_{\text{eff}} L/2) \exp(-j\beta_{\text{eff}} L), \quad (1)$$

where, $E_{\text{out}}(\omega)$ and $E_{\text{ref}}(\omega)$ are the complex electric fields at angular frequency ω on the entrance and exit of the fiber, respectively; T_1 and T_2 are the total transmission coefficients at the entrance and exit faces, respectively; C is the coupling coefficient, the same for the entrance and exit faces; β_{eff} is the propagation constant of the fundamental mode; α_{eff} is the effective material loss that the propagating mode experiences; and L is the fiber length.

At least two different lengths of a fiber are required to determine the THz properties (α_{eff} and β_{eff}) of the fiber from the measured output power (Eq. (1)). Applying Eq. (1) to two different lengths (L_1 and L_2), the transfer function determined from the ratio of $E_{out1}(\omega)$ and $E_{out2}(\omega)$ reads as [14]:

$$E_{out1}(\omega)/E_{out2}(\omega) = \exp(-\alpha_{eff}(L_1 - L_2)/2)\exp(-j\beta_{eff}(L_1 - L_2)) \ . \quad (2)$$

Then α_{eff} and β_{eff} of the fiber is obtained form the amplitude and the phase of Eq. (2). The C, T_1 and T_2 coefficients are canceled provided that a cut back measurement is carried out. This is essential for the fiber loss measurement, but not for the effective refractive index measurement.

Unlike the glass which is brittle, polymer is elastic. This makes porous polymer fibers mechanically soft resulting in non-trivial cleaving methods [15]. At this stage, it is not possible to conduct on spot cleaving when the fiber is situated in the system. Therefore, three different lengths of each fiber are considered to determine the THz properties of microwire, spider-web and rectangular porous fibers. In this method, the effective refractive index of the fibers, which depends on the phase of the transfer function in Eq. (2), can be determined without any uncertainty.

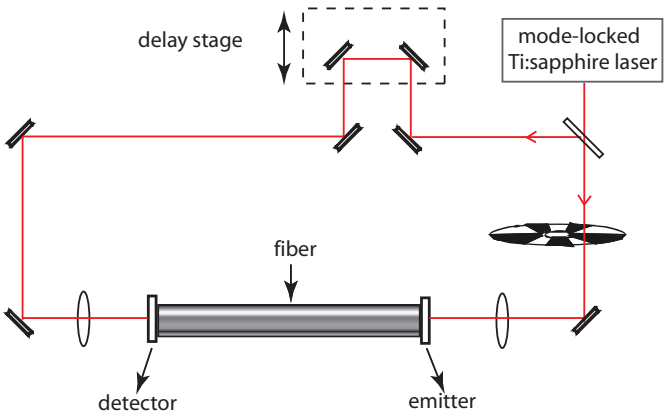

Fig. 2: Schematic of the THz-TDS setup.

The effective refractive index (n_{eff}) for the fibers is determined by comparing the output electric fields of each pair of the three scans. Then, the three individual effective refractive indices obtained from comparison are averaged. The measured and theoretically calculated effective refractive index of the spider-web porous fiber and microwire are shown in Fig. 3(a). The SEM image of the cross-section of the fabricated porous fiber, Fig. 1(c), is used for the numerical modeling. The three fiber lengths used for the spider-web porous fiber are 24.9, 20.4 and 16.0 mm and for the microwire are 25.0, 20.2 and 17.7 mm. As shown in Fig. 3(a), the measurements agree well with the expected theoretical results. Experimental results validate that the refractive index of porous fiber is a flatter function of frequency compared to that of the microwire, which corresponds to a lower dispersion. As the frequency increases, most of the guided power of the microwire is transferred to the solid core, while most of the guided power of the porous fiber is transferred to the sub-wavelength air-hole regions. This results in a lower dispersion characteristic for the porous fiber compared with the microwire.

Here, we consider two major sources of errors: fiber length and data processing uncertainties. A ±0.1 mm variation is considered for the length uncertainty. In order to remove the low-frequency *1/f* noise two techniques have been used, which are base line removal and high pass filtering. The difference between these methods and the effect of variation of the cut-off frequency of the high pass filter are considered as the source of data processing uncertainty. The error bars shown in Fig. 3(a) represent the quadrature sum of standard deviations obtained from two sources of uncertainty.

Fig. 3(b) shows the experimentally measured refractive indices of the *x*- and *y*-polarization modes for the rectangular porous fiber together with the theoretically calculated values based on the SEM image of the cross-section of the fabricated porous fiber, Fig. 1(f). The three fiber lengths used for the rectangular porous fiber are 30.0, 34.1 and 38.2 mm. As it can be seen, a 0.012 birefringence is achieved for 0.65 THz which is comparable to the expected theoretical results. Unsurprisingly the measured n_{eff} of the rectangular porous fiber is flatter function of frequency compared to spider-web porous fiber due to it's higher porosity value.

It is worth mentioning that the difference between the experimental and theoretical values at lower effective refractive index values is most likely due to the slight bending of the fibers. Due to the week confinement of the mode, the power is lost as radiation.

Conclusion: In conclusion, two types of THz polymer porous fibers—spider-web and rectangular porous fibers—have been fabricated. These fabricated fibers have high porosity of 57% and 65%,

respectively. The effective refractive index measured by terahertz time domain spectroscopy shows a good agreement between the theoretical and experimental results. This verifies experimentally the low dispersion characteristics of the THz porous fiber. A birefringence of 0.012 at 0.65 THz is also observed for rectangular porous fiber.

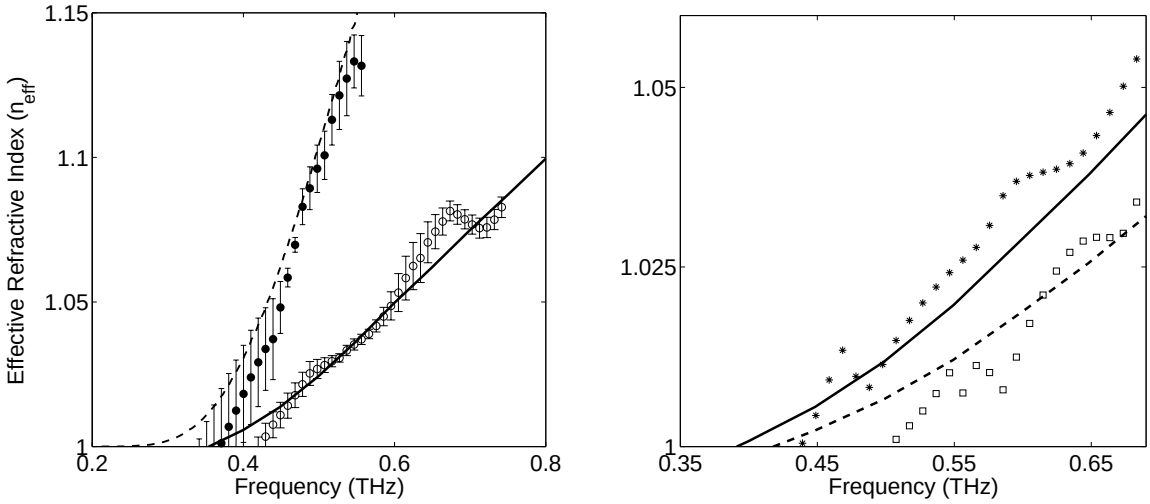

(a) (b)

Fig. 3: (a) Experimentally measured effective refractive index of a 350 μm diameters of spider-web porous fiber (circles), a 250 μm diameter microwire (dots). Theoretical calculated results based on the SEM images of a 350 μm diameters of spider-web porous fiber (solid line), a 250 μm diameter microwire (dashed line). (b) Experimentally measured effective refractive index of a 350 μm diameter of rectangular porous fiber x-polarization (stars) and y-polarization (squares). Theoretical calculated results based on the SEM image of the rectangular porous fiber x-polarization (solid line) and y-polarization (dashed line).

Acknowledgment: This research was supported under the Australian Research Council's (ARC) Discovery Projects funding scheme (project numbers DP0556112 and DP0880436), Australian Research Council Nanotechnology Network (ARCNN) Overseas Travel Fellowship and Adelaide University Research Abroad Scholarship. The authors gratefully acknowledge Markus Wächter from Institut für Halbleitertechnik at RWTH Aachen University for assistance with THz hardware. T. Monro acknowledges the support of an ARC Federation Fellowship.

References

1. L.-J. Chen, H.-W. Chen, T.-F. Kao, J.-Y. Lu, and C.-K. Sun, *Optics Letters* **31**, pp. 308–310 (2006).
2. S. Afshar Vahid, S. Atakaramians, B. M. Fischer, H. Ebendorff- Heidepriem, T. M. Monro, and D. Abbott, *CLEO/QELS*, p. JWA105 (2007).
3. W. Withayachumnankul, G. M. Png, X. Yin, S. Atakaramians, I. Jones, H. Lin, B. Ung, J. Balakrishnan, B.W.-H. Ng, B. Ferguson, S. P. Mickan, B. M. Fischer, and D. Abbott, *Proceedings of the IEEE* **95**, pp. 1528–1558 (2007).
4. J.-Y. Lu, C.-P. Yu, H.-C. Chang, H.-W. Chen, Y.-T. Li, C.-L. Pan, and C.-K. Sun, *Applied Physics Letters* **92**, 064105 (2008).
5. K. Nielsen, H. K. Rasmussen, A. J. L. Adam, P. C. M. Planken, O. Bang, and P. U. Jepsen, *Optics Express* **17**, pp. 8592–8601 (2009).
6. B. Bowden, J. A. Harrington, and O. Mitrofanov, *Optics Letters* **32**, pp. 2945–2947 (2007).
7. A. Hassani, A. Dupuis, and M. Skorobogatiy, *Applied Physics Letters* **92**, 071101 (2008).
8. S. Atakaramians, S. Afshar Vahid, B. M. Fischer, D. Abbott, and T. M. Monro, *Optics Express* **16**, pp. 8845–8854 (2008).
9. S. Atakaramians, S. Afshar, B. M. Fischer, D. Abbott, and T. M. Monro, *Optics Communications* **282**, pp. 36–38 (2008).
10. A. Dupuis, J.-F. Allard, D. Morris, K. Stoeffler, C. Dubois and M. Skorobogatiy, *Optics Express* **17**, pp. 8012–8028 (2009).
11. H. Ebendorff-Heidepriem and T. M. Monro, *Optics Express* **15**, pp. 15,086–15,096 (2007).
12. H. Ebendorff-Heidepriem, T. M. Monro, M. A. van Eijkelenborg, and M. C. J. Large, *Optics Communications* **273**, pp. 133–137 (2007).
13. M. Wächter, M. Nagel, and H. Kurz, *Applied Physics Letters* **90**, 061111 (2007).
14. D. Grischkowsky, *IEEE Journal on selected topics in Quntum Electronics* **6**, pp. 1122-1135 (2000).
15. S. Atakaramians, S. Afshar Vahid, H. Ebendorff-Heidepriem, M. Nagel, B. M. Fischer, D. Abbott, and T. M. Monro, *Optics Express*, submitted.